GLOBAL JOURNAL OF ENGINEERING RESEARCH VOL. 3, No. 1 & 2, 2004: 21 - 37
COPYRIGHT(C) BACHUDO SCIENCE CO. LTD. PRINTED IN NIGERIA. ISSN 1596-292X

ANALYSIS OF ELECTRICAL - THERMAL COUPLING OF INDUCTION MACHINE.

O. I. OKORO

(Received 17 July 2003; Revision Accepted 29 September 2003)

ABSTRACT

The interaction of the Electrical and mechanical parts of Electrical machines gives rise to the heating of the machine's constituent parts. This consequently leads to an increase in temperature which if not properly monitored may lead to the breakdown of the machine. This paper therefore presents the Electrical and thermal coupling of induction machine in order to study its mechanical and electrical transient behaviours at run-up condition. The analysis of the coupled system is represented in state variable form with currents and temperatures of the machine parts as its variables. The proposed electrical - thermal coupling of induction machine is simulated.

KEYWORDS: Thermal Network, Simulation, Induction machine, Mechanical model, Lumped parameter.

INTRODUCTION

The past works on induction machine transients have demonstrated how the Electrical and Mechanical models of the machine can be developed (Krause and Thomas 1965, Jordan 1967, Smith 1996). Unfortunately, these works lack in their ability to explore the thermal behaviour of the machine as well as simultaneously predict the dynamic behaviour of the machine due to Electrical and Mechanical transients. In a situation where the temperature rise of the machine parts is to be monitored and the mechanical speed regulated, it becomes necessary to look at the overall models of the induction machine. In the proposed coupled model, the electrical model generates the electromagnetic torque which is fed into the mechanical model. The mechanical model produces the power losses which the thermal model needs in order to predict the motor tempratures. The motor tempratures which are generated from the thermal model is fed into the electrical model since the rotor and stator resistances are temperature dependent. Figure 1 illustrates the block diagram of the coupled model.

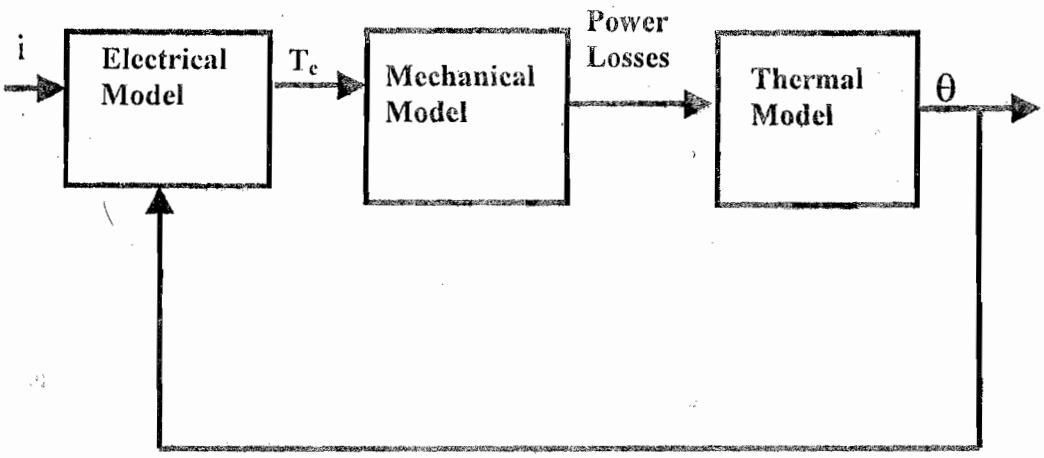

Figure 1: Block diagram of the proposed coupled system.

In(Bastos, Cabreira, Sadowski and Arrunda 1997) a thermal analysis of induction motors using a weak coupled modelling has been developed. The authors used finite element method in the analysis of the thermal model. The demerit of this method lies on the fact that three- dimensional and time- dependent problems are generally involving both in software development and hardware implementation(Kylander 1995, Chan, Yan, Chen, Wang, Zezhong and Chau 1994). Again, it lacks in flexibility in handling complex boundary conditions and geometry(Rajagopal, Seetharamu and Ashwathnarayana 1998). In this paper, the lumped parameter model, otherwise known as the thermal network model is applied in the modelling of the

O. I. OKORO, Department of Electrical Engineering, University of Nigeria, Nsukka - Nigeria

thermal model of the coupled system. The merit of the thermal network parameters can be derived from entirely dimensional information, the thermal properties of the materials used in designing the machine, and the constant heat trnsfer coefficients. This feature makes the model to be easily adapted to a range of machine sizes(Mellor, Roberts and Turner 1995). The electrical model of the machine is first developed followed by the mechanical model. The paper continues with the thermal modelling and the state variable analysis of the coupled system. Lastly, the computer simulation and results as well as the concluding remarks are presented.

ELECTRICAL MODEL

The differential equations governing the transient performance of the induction machine can be described in several ways and they only differ in detail and in their suitability for use in a given application. The conventional machine model is developed using the traditional method of reducing the machine to a two-axis coil(d-q axis) model on both the stator and the rotor as described by Krause and Thomas,(1965). The d-q axis model of the motor provides a convenient way of modelling the machine and is most suitable for numerical solution.

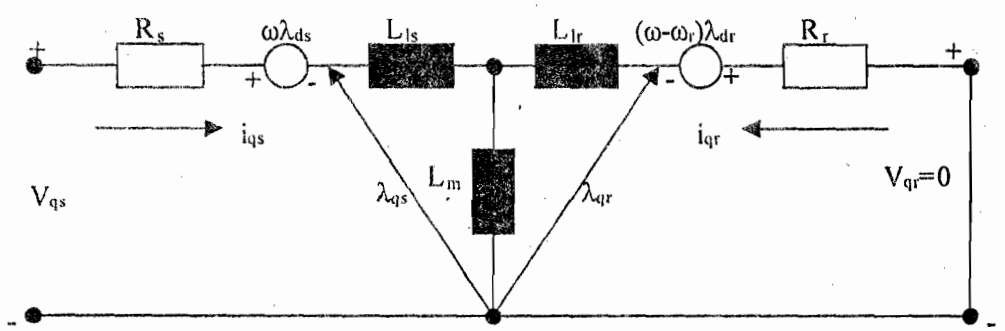

Figure 2a

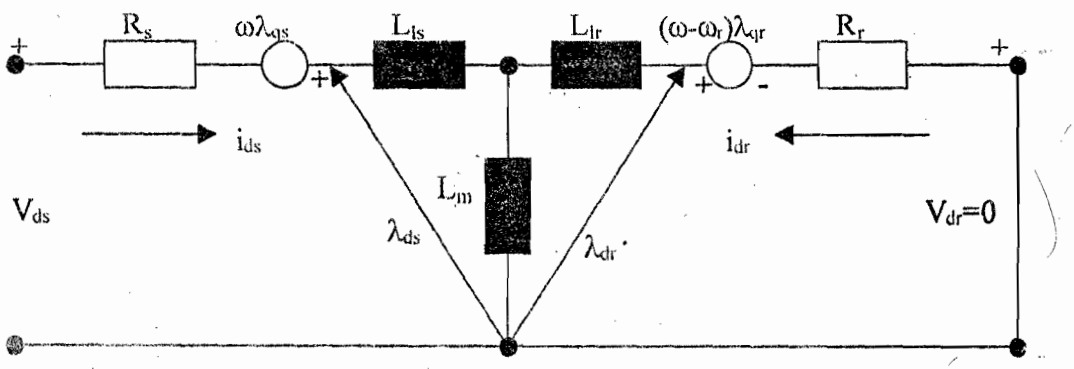

Figure.2b

Figure 2: Squirrel-Cage Induction machine models in d-q axis: (a) q-axis model (b) d-axis model.

This is preferable to the space-vector machine model which describes the machine in terms of complex variables(Vas 1992). Figure 2 shows the d-q equivalent circuits for a 3-phase, symmetrical squirrel-cage induction machine in arbitrary-reference frame with the zero-sequence component neglected. The non-linear differential equations which describe the dynamic performance of an ideal symmetrical Induction machine in an arbitrary reference frame could be derived from the d-q equivalent circuits as in Krause and Thomas,(1965).

$$\begin{bmatrix} V_{qs} \\ V_{ds} \\ 0 \\ 0 \end{bmatrix} = \begin{bmatrix} (R_s + L_s p) & \omega L_s & L_m p & \omega L_m \\ -\omega L_s & (R_s + L_s p) & -\omega L_m & L_m p \\ L_m p & (\omega - \omega_r) L_m & (R_r + L_r p) & (\omega - \omega_r) L_r \\ -(\omega - \omega_r) L_m & L_m p & -(\omega - \omega_r) L_r & (R_r + L_r p) \end{bmatrix} \begin{bmatrix} i_{qs} \\ i_{ds} \\ i_{qr} \\ i_{dr} \end{bmatrix} \quad (1)$$

where,

$$L_s = L_{ls} + L_m \tag{2}$$

$$L_r = L_{lr} + L_m \tag{3}$$

$$p = \frac{d}{dt} \tag{4}$$

Under balanced condition, the stator voltages of a three-phase induction machine may be considered as sinusoidal and expressed as

$$V_{as} = \sqrt{2}V \cos \omega_b t \tag{5}$$

$$V_{bs} = \sqrt{2}V \cos\left(\omega_b t - \frac{2\pi}{3}\right) \tag{6}$$

$$V_{cs} = \sqrt{2}V \cos\left(\omega_b t + \frac{2\pi}{3}\right) \tag{7}$$

These stator voltages are related to the d-q frame of reference by Krause and Thomas,(1965).

$$\begin{bmatrix} V_{sq} \\ V_{sd} \\ V_o \end{bmatrix} = [C] \begin{bmatrix} V_{as} \\ V_{bs} \\ V_{cs} \end{bmatrix} \tag{8}$$

Also, the d-q stator currents have to be transformed to the three phase stator currents as

$$\begin{bmatrix} i_{sq} \\ i_{sd} \\ i_0 \end{bmatrix} = [C] \begin{bmatrix} i_{sa} \\ i_{sb} \\ i_{sc} \end{bmatrix} \tag{9}$$

$$\begin{bmatrix} i_{sa} \\ i_{sb} \\ i_{sc} \end{bmatrix} = [C]^{-1} \begin{bmatrix} i_{sq} \\ i_{sd} \\ i_0 \end{bmatrix} \tag{10}$$

where,

$$[C] = \frac{2}{3} \begin{bmatrix} \cos\theta & \cos\left(\theta - \frac{2\pi}{3}\right) & \cos\left(\theta - \frac{4\pi}{3}\right) \\ \sin\theta & \sin\left(\theta - \frac{2\pi}{3}\right) & \sin\left(\theta - \frac{4\pi}{3}\right) \\ \frac{1}{2} & \frac{1}{2} & \frac{1}{2} \end{bmatrix} \tag{11}$$

$$[C]^{-1} = \begin{bmatrix} \cos\theta & \sin\theta & 1 \\ \cos\left(\theta - \frac{2\pi}{3}\right) & \sin\left(\theta - \frac{2\pi}{3}\right) & 1 \\ \cos\left(\theta - \frac{4\pi}{3}\right) & \sin\left(\theta - \frac{4\pi}{3}\right) & 1 \end{bmatrix} \quad (12)$$

The Electromagnetic torque, T_e is given by Krause,(1986) as:

$$T_e = \frac{3}{2} PL_m \left(i_{qs} i_{dr} - i_{ds} i_{qr}\right) \quad (13)$$

where, P= Number of pole pairs.
The test machine electrical parameters used in the simulation are determined by carrying out D.C. measurement test, No-Load test, Blocked-rotor test and retardation test on the machine. The machine parameters are recorded in Appendix A.

MECHANICAL MODEL

The mechanical model of an induction motor comprises of the equations of motion of the motor and driven load as shown in figure 3 and is usually represented as a second-order differential equation(Smith 1990).

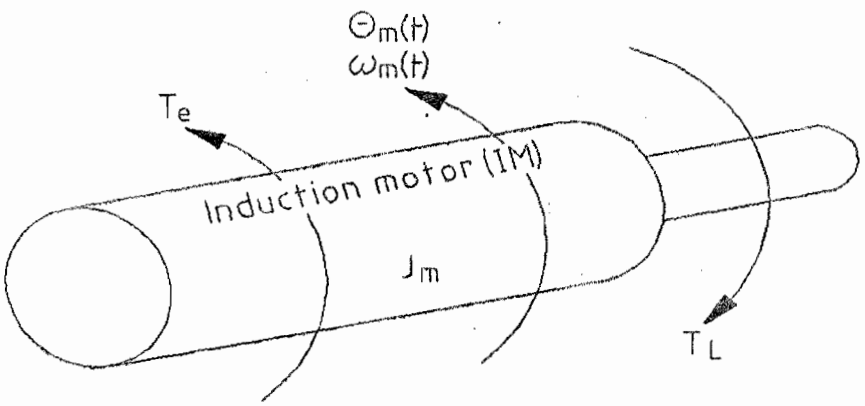

Figure 3: Motor mechanical model schematic

$$J_m p^2 \theta_m = T_e - T_L \quad (14)$$

Decomposing equation(14) into two first-order differential equations gives,

$$p\theta_m = \omega_m \quad (15)$$

$$J_m\left(p\omega_m\right) = \left(T_e - T_L\right) \quad (16)$$

But,

$$\omega = \omega_m P \quad (17)$$

$$\theta_r = \theta_m P \quad (18)$$

where,

ω_m = angular velocity of the rotor

θ_m = rotor angular position

θ_r = electrical rotor angular position

ω_r = electrical angular velocity

J_m = combined rotor and load inertia coefficient

T_L = applied load torque

THERMAL MODEL

The thermal network model for the squirrel-cage induction machine is developed according to the principles reported by Okoro, (2002). Figure 4 shows the typical construction of a Squirrel-Cage induction machine. In developing the thermal network model, the machine geometry is divided into basic elements and each element being identified by a node in the thermal network with its corresponding thermal capacitance and heat source. The choice of subdividing a machine into elementary components remains a compromise between the simplicity of the model and the accuracy required of the results (Bousbaine, McCormick and Low, 1995). It has been shown by Kylander,(1995) that high level of accuracy could be achieved by modest subdivision of the induction machines geometrical parts. The developed thermal network model is shown in figure56. The model consists of 11nodes and 15 thermal resistances. In the model, the stator of the machine has networks for the stator iron, stator winding and the end windings. It is assumed that the heat transfer from the rotor winding through the air-gap goes directly to the stator winding with negligible impact on the stator teeth. The rotor part of the machine is divided into the rotor iron, rotor winding and the end rings. By connecting the networks for the rotor, stator and frame together, the thermal network model for the machine is realised. The values of the thermal resistances and capacitances are shown in Appendix B.

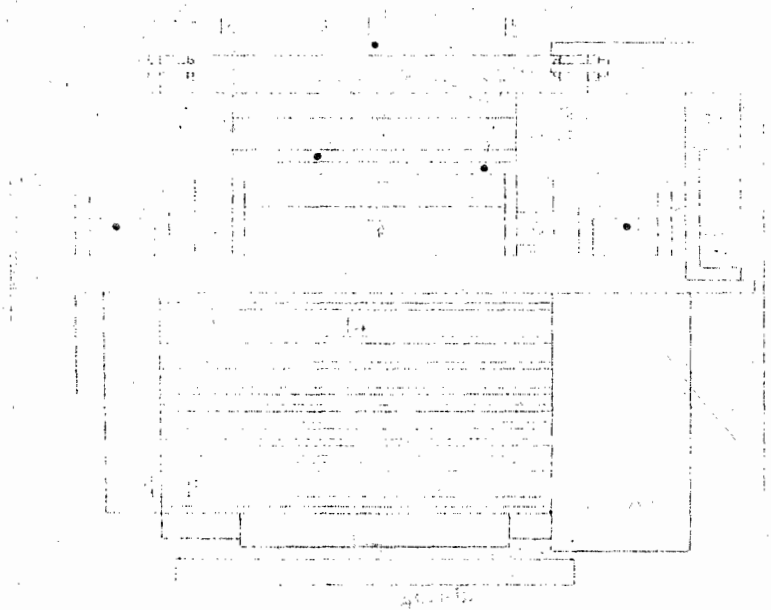

Figure 4: Typical Construction of Squirrel-Cage Induction Machine.

1. Frame	6. Rotor iron	11.,12. Bearing	16. Stator teeth
2. Stator iron	7. Rotor winding	13. Fan	17. Shaft
3. Stator winding	8.,9. Endrings	14. Cooling ribs	
4.,5. End windings	10. Ambient air	15. Air gap	

The transient thermal network equations for the thermal model taken node by node give:

$$\frac{d\theta_1}{dt} = \frac{1}{C_1}\left(P_1 - \frac{1}{R_{1b}}(\theta_1 - \theta_{kb}) - \frac{1}{R_{12}}(\theta_1 - \theta_2)\right) \quad (19)$$

$$\frac{d\theta_2}{dt} = \frac{1}{C_2}\left(P_2 - \frac{1}{R_{12}}(\theta_2 - \theta_1) - \frac{1}{R_{23}}(\theta_2 - \theta_3) - \frac{1}{R_{26}}(\theta_2 - \theta_6)\right) \quad (20)$$

$$\frac{d\theta_3}{dt} = \frac{1}{C_3}\left(P_3 - \frac{1}{R_{23}}(\theta_3 - \theta_2) - \frac{1}{R_{35}}(\theta_3 - \theta_5) - \frac{1}{R_{34}}(\theta_3 - \theta_4)\right) \quad (21)$$

$$\frac{d\theta_4}{dt} = \frac{1}{C_4}\left(P_4 - \frac{1}{R_{34}}(\theta_4 - \theta_3) - \frac{1}{R_{410}}(\theta_4 - \theta_{10})\right) \quad (22)$$

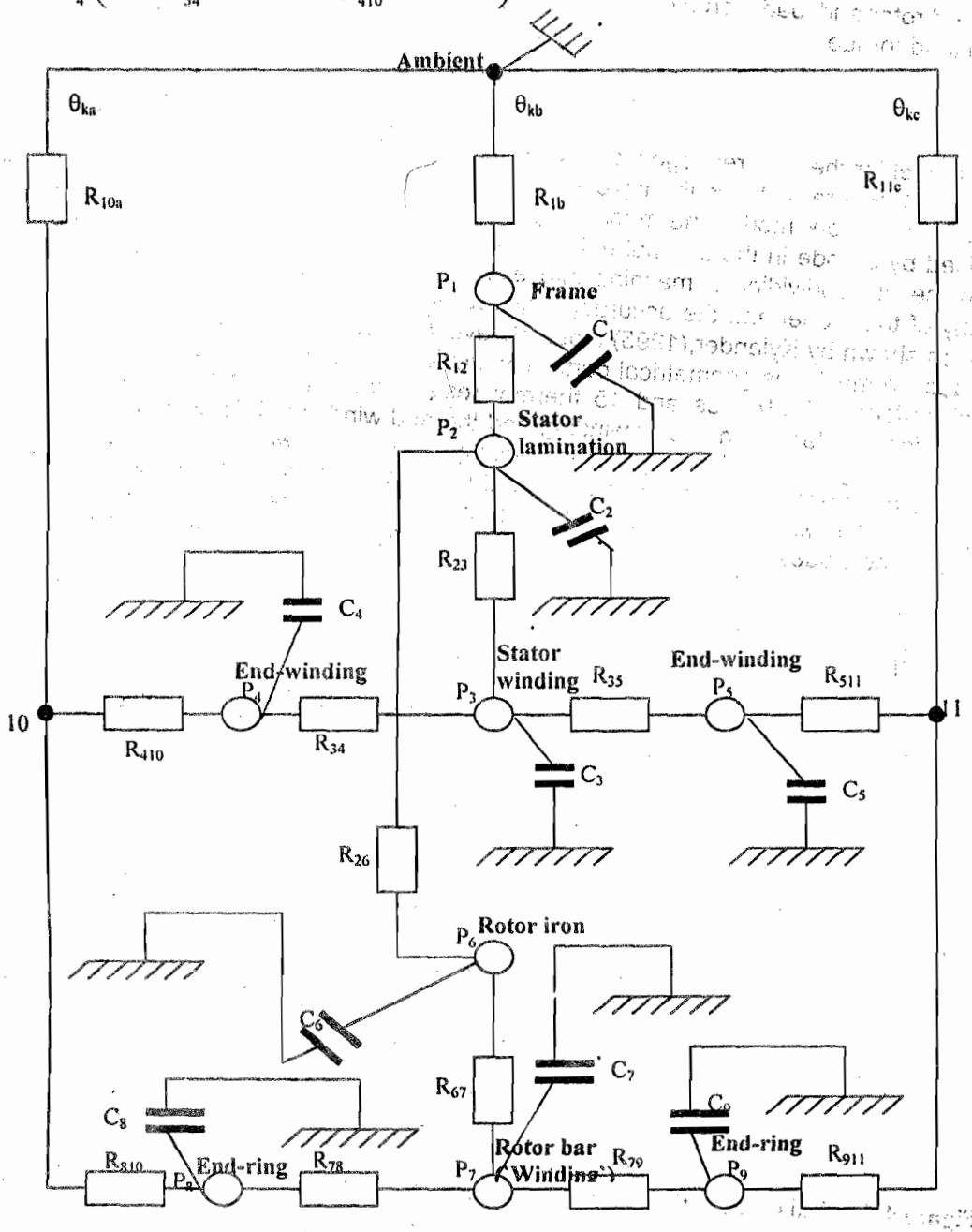

Figure 5: Thermal network model representation for the 7.5KW induction machine.

$$\frac{d\theta_5}{dt}=\frac{1}{C_5}\left(P_5-\frac{1}{R_{51}}(\theta_5-\theta_{11})-\frac{1}{R_{35}}(\theta_5-\theta_3)\right) \quad (23)$$

$$\frac{d\theta_6}{dt}=\frac{1}{C_6}\left(P_6-\frac{1}{R_{26}}(\theta_6-\theta_2)-\frac{1}{R_{67}}(\theta_6-\theta_7)\right) \quad (24)$$

$$\frac{d\theta_7}{dt}=\frac{1}{C_7}\left(P_7-\frac{1}{R_{79}}(\theta_7-\theta_9)-\frac{1}{R_{78}}(\theta_7-\theta_8)-\frac{1}{R_{67}}(\theta_7-\theta_6)\right) \quad (25)$$

$$\frac{d\theta_8}{dt}=\frac{1}{C_8}\left(P_8-\frac{1}{R_{78}}(\theta_8-\theta_7)-\frac{1}{R_{810}}(\theta_8-\theta_{10})\right) \quad (26)$$

$$\frac{d\theta_9}{dt}=\frac{1}{C_9}\left(P_9-\frac{1}{R_{911}}(\theta_9-\theta_{11})-\frac{1}{R_{79}}(\theta_9-\theta_7)\right) \quad (27)$$

$$\frac{d\theta_{10}}{dt}=\frac{1}{C_{10}}\left(P_{10}-\frac{1}{R_{410}}(\theta_{10}-\theta_4)-\frac{1}{R_{810}}(\theta_{10}-\theta_8)-\frac{1}{R_{10a}}(\theta_{10}-\theta_{ka})\right) \quad (28)$$

$$\frac{d\theta_{11}}{dt}=\frac{1}{C_{11}}\left(P_{11}-\frac{1}{R_{511}}(\theta_{11}-\theta_5)-\frac{1}{R_{911}}(\theta_{11}-\theta_9)-\frac{1}{R_{11c}}(\theta_{11}-\theta_{kc})\right) \quad (29)$$

In the model, the power losses are given as input values. The ohmic losses of the stator and rotor are expressed mathematically by

$$P_{cu1}(t,\theta_{1cu})=R_1(\theta_{1cu}(t))\left[i_{ds}^{\,2}(t)+i_{qs}^{\,2}(t)\right] \quad (30)$$

$$P_{cu2}(t,\theta_{2cu})=R_2(\theta_{2cu}(t))\left[i_{dr}^{\,2}(t)+i_{qr}^{\,2}(t)\right] \quad (31)$$

From equations(30-31), it can be seen that the stator and rotor resistances are dependent on the motor temperature. Therefore, the measured resistance at room temperature(θ_0) must be corrected to a specified temperature(θ). The correction for the resistance change with temperature can be made by

$$R = R_{20}\frac{K+\theta}{K+\theta_0} \quad (32)$$

Where R is the corrected resistance at θ, and K is equal to 245 for Aluminium and 235 for Copper.

The iron losses in the test machine can be broadly divided into three:

- Iron losses in the machine yoke, P_{Fe1Y}
- Iron losses in the stator teeth, P_{Fe1T}
- Iron losses in the rotor, P_{Fe2R}

The hysteresis losses, according to Steinmetz law are proportional to frequency and to $B_{max}^{(1.5\text{-}2.5)}$ depending on magnetic saturation. The eddy current losses are proportional to the square of the frequency and also to the square of the maximum value of flux density. The empirical form of these losses is given by Klamt, (1962) as:

$$P_H = \sigma_H \frac{f}{100} B^2 m \quad (33)$$

$$P_E = \sigma_E \left(\Delta_{Fe} \frac{f}{100} B \right)^2 m \quad (34)$$

$$P_{Fe} = P_H + P_E = \left[\sigma_H \frac{100}{f} + \sigma_E \Delta_{Fe}^{\ 2} \right] \left(\frac{f}{100} \right)^2 B^2 m \quad (35)$$

where,

σ_H =Hysteresis loss Coefficient

σ_E =Eddy-current loss Coefficient

Δ_{Fe} =the thickness of the lamination sheet

m = mass

f = frequency

B = magnetic flux density

The total iron losses, P_{FeT} becomes,

$$P_{FeT} = P_{Fe1Y} + P_{Fe1T} + P_{Fe2R} \quad (36)$$

$$P_{FeT} = \underbrace{P_{FeHY} + P_{FeEY}}_{P_{Fe1Y}} + \underbrace{P_{FeHT} + P_{FeET}}_{P_{Fe1T}} + \underbrace{P_{FeH2R} + P_{FeE2R}}_{P_{Fe2R}} \quad (37)$$

The parameters σ_H, σ_E and m in equations(33-34) are material dependent and can be eliminated by normalizing the equations and expressing the iron losses as factors dependent only on magnetic flux and frequency.

$$\frac{P_H}{P_{NH}} = \frac{\sigma_H \frac{f}{100} B^2 m}{\sigma_H \frac{f_N}{100} B^2{}_N m} = \frac{f}{f_N} \left(\frac{\psi}{\psi_N} \right)^2 \quad (38)$$

$$\frac{P_E}{P_{NE}} = \frac{\sigma_E \left(\Delta_{Fe} \frac{f}{100} B \right)^2 m}{\sigma_E \left(\Delta_{Fe} \frac{f_N}{100} B_N \right)^2 m} = \left(\frac{f}{f_N} \right)^2 \left(\frac{\psi}{\psi_N} \right)^2 \quad (39)$$

where,

$$\frac{B}{B_N} = \frac{A_{eff} \psi}{A_{eff} \psi_N} = \frac{\psi}{\psi_N} \quad (40)$$

ψ = magnetic flux
ψ_N = rated magnetic flux
A_{eff} = effective Area
f_N = rated frequency

The magnetic flux in the stator and rotor can be expressed respectively as,

$$\psi_1 = \sqrt{\psi^2_{1d} + \psi^2_{1q}} \quad (41)$$

$$\psi_2 = \sqrt{\psi^2_{2d} + \psi^2_{2q}} \quad (42)$$

Application of equations(38-39) requires that the machine's rated stator and rotor frequency as well as the rated iron losses in equation(37) be determined. The determination of these rated losses of the machine can be achieved by subdividing the total rated iron losses in the manner reported by Rohrmoser ,(1998):

1. A factor K_S is used to distribute the total iron losses between the stator and the rotor.

$$P_{Fe1} = K_S P_{FeT} \quad (43)$$

$$P_{Fe2R} = P_{Fe2} = (1 - K_S) P_{FeT} \quad (44)$$

2. The stator iron losses are further distributed between the teeth and the yoke with a factor K_T.

$$P_{Fe1Y} = K_T P_{Fe1} \quad (45)$$

$$P_{Fe1T} = (1 - K_T) P_{Fe1} \quad (46)$$

3. The calculated losses in (1) and (2) can now be shared between hysteresis and Eddy-current losses using the three constant factors, H_Y, H_T and H_R.

$$P_{FeH1Y} = H_Y P_{Fe1Y} \quad (47)$$

$$P_{FeE1Y} = (1 - H_Y) P_{Fe1Y} \quad (48)$$

$$P_{FeH1T} = H_T P_{Fe1T} \quad (49)$$

$$P_{FeE1T} = (1 - H_T) P_{Fe1T} \quad (50)$$

$$P_{FeH2R} = H_R P_{Fe2R} \quad (51)$$

$$P_{FeE2R} = (1 - H_R) P_{Fe2R} \quad (52)$$

The rotor frequency is expressed as

$$f_2 = f_s = f_1 - f \tag{53}$$

By substituting equations (43-52), into equations(38) and (39), the below equations result.

$$P_{FeH1Y} = H_Y K_T K_S P_{NFeT} \frac{f_1}{f_{1N}} \left(\frac{\psi_1}{\psi_{1N}} \right)^2 \tag{54}$$

$$P_{FeE1Y} = (1 - H_Y) K_T K_S P_{NFeT} \left(\frac{f_1}{f_{1N}} \right)^2 \left(\frac{\psi_1}{\psi_{1N}} \right)^2 \tag{55}$$

$$P_{FeH1T} = H_T (1 - H_T) K_S P_{NFeT} \frac{f_1}{f_{1N}} \left(\frac{\psi_1}{\psi_{1N}} \right)^2 \tag{56}$$

$$P_{FeE1T} = (1 - H_T)(1 - K_T) K_S P_{NFeT} \left(\frac{f_1}{f_{1N}} \right)^2 \left(\frac{\psi_1}{\psi_{1N}} \right)^2 \tag{57}$$

$$P_{FeH2R} = H_R (1 - K_S) P_{NFeT} \left(\frac{f_2}{f_{2N}} \right) \left(\frac{\psi_2}{\psi_{2N}} \right)^2 \tag{58}$$

$$P_{FeE2R} = (1 - H_R)(1 - K_S) P_{NFeT} \left(\frac{f_2}{f_{2N}} \right)^2 \left(\frac{\psi^2}{\psi_{2N}} \right)^2 \tag{59}$$

The loss distribution factors K_S, K_T, H_Y, H_T and H_R differ for different machines depending on construction and the material used and can be obtained from the manufacturer's data or from experiment. For the test machine, these factors lie between 0.3 to 0.99.
The stray load losses, which represent about 1.8% of the machine rated power as reported by The IEEE Standard, (1991), are taken into consideration and added to the rotor losses.

COMPUTER SIMULATION

In order to validate the accuracy of the proposed coupled models, it becomes necessary to predict the dynamic behaviour of the test machine under run-up condition. The proposed coupled models give rise to a set of differential equations which describe both the Electrical and Thermal models of the machine. MATLAB© m- files (The MATLAB 1997) are developed for half of the machine(i.e. for the thermal model) in order to determine the average temperature rise of the various parts of the machine. This reduces the set of differential equations for the thermal model to eight. These equations are solved simultaneously with the Electrical and Mechanical models equations using Runge-Kutta numerical method. By incorporating the ambient temperature and assuming that the rotor and stator currents are initially at zero, the time function of the power losses, temperature rise of the machine parts, mechanical rotor speed, electromagnetic torque, stator resistance, rotor resistance and stator phase currents can be predicted with the load applied at 0.5s. Figure 6 shows the time function of the rotor speed, electromagnetic torque and the mechanical rotor speed. The graph of the rotor speed against time shows that the machine speed falls below the rated speed as the load is applied at t equals 0.5s.

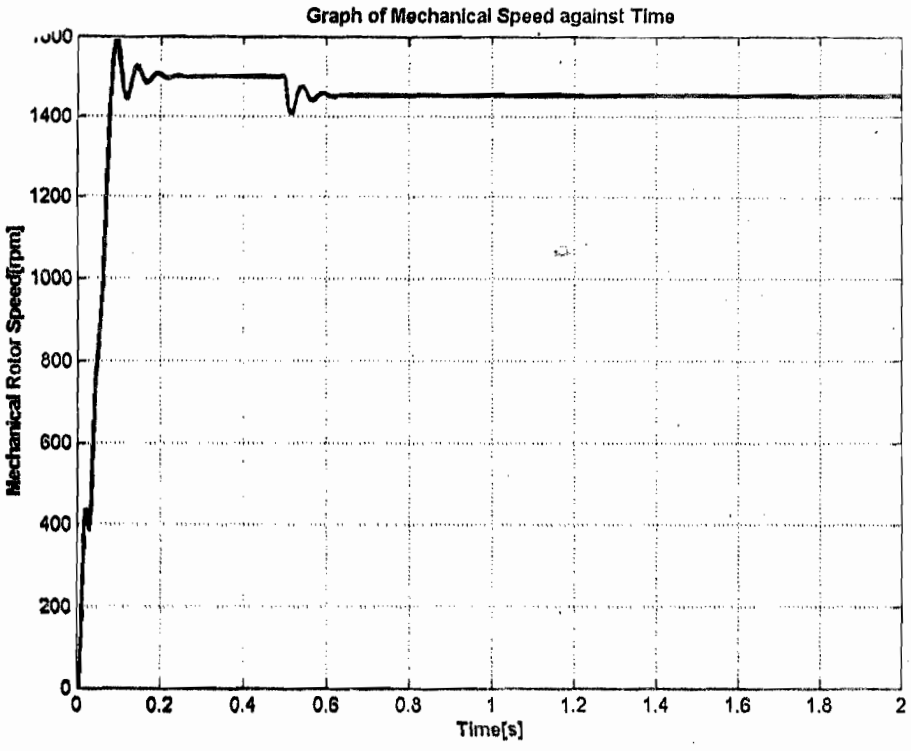

Figure 6a: Mechanical Rotor Speed – Time Curve

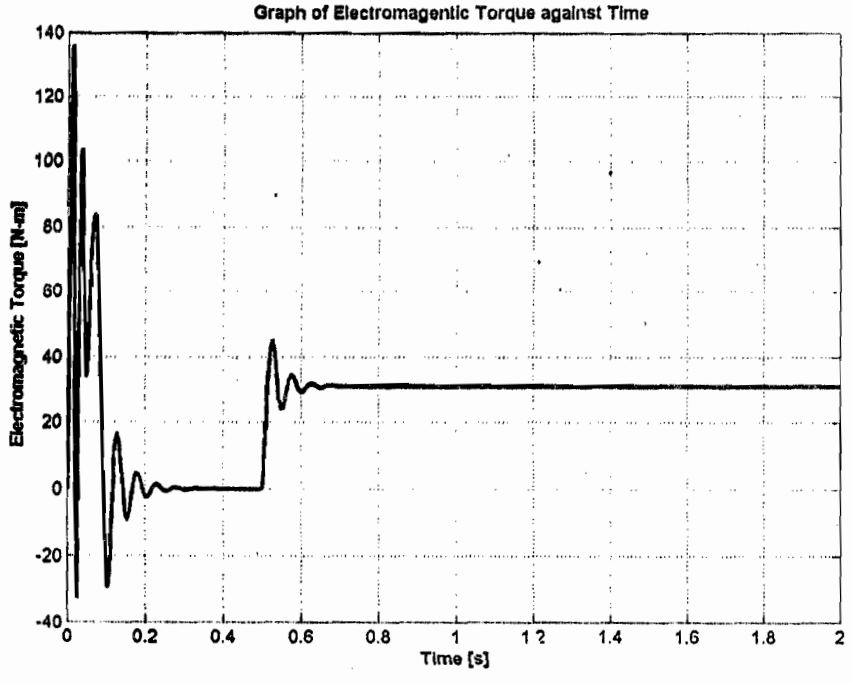

Figure 6b: Electromagnetic Torque – Time Curve

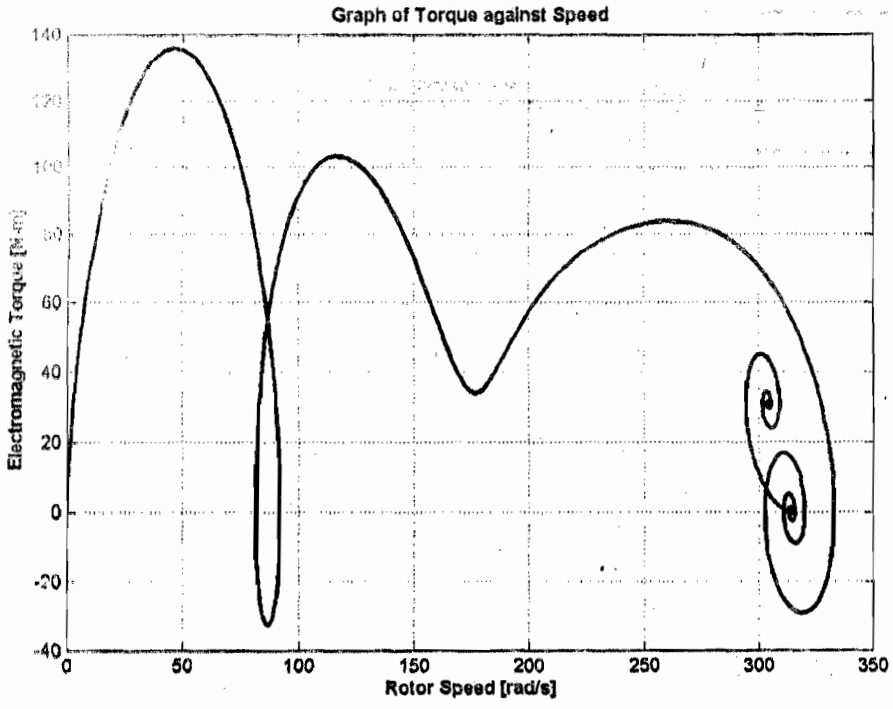

Figure 6c: Electromagnetic Torque – Rotor Speed
Figure 6: Transient performance of the test machine at run-up condition.

The reverse is the case for the electromagnetic torque-time graph where the developed torque rises sharply to the value of the applied load. Figure 7 shows the graph of temperature rise against time for the stator lamination, frame, stator winding and end-winding.

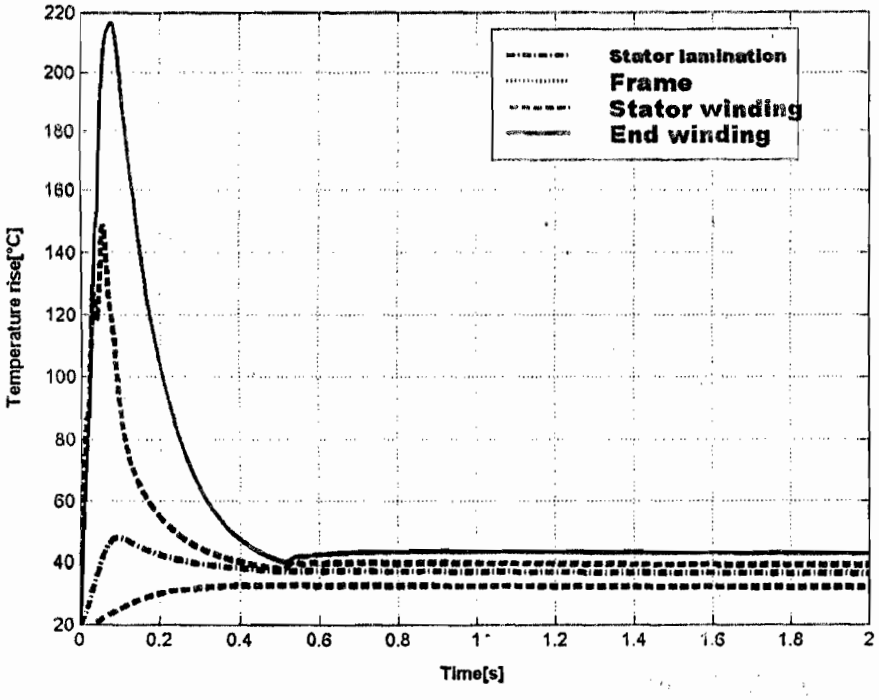

Figure 7: Graph of Temperature rise against Time.

Figure 8 shows the time function of the temperature rise in the rotor bar, rotor iron and the end ring.

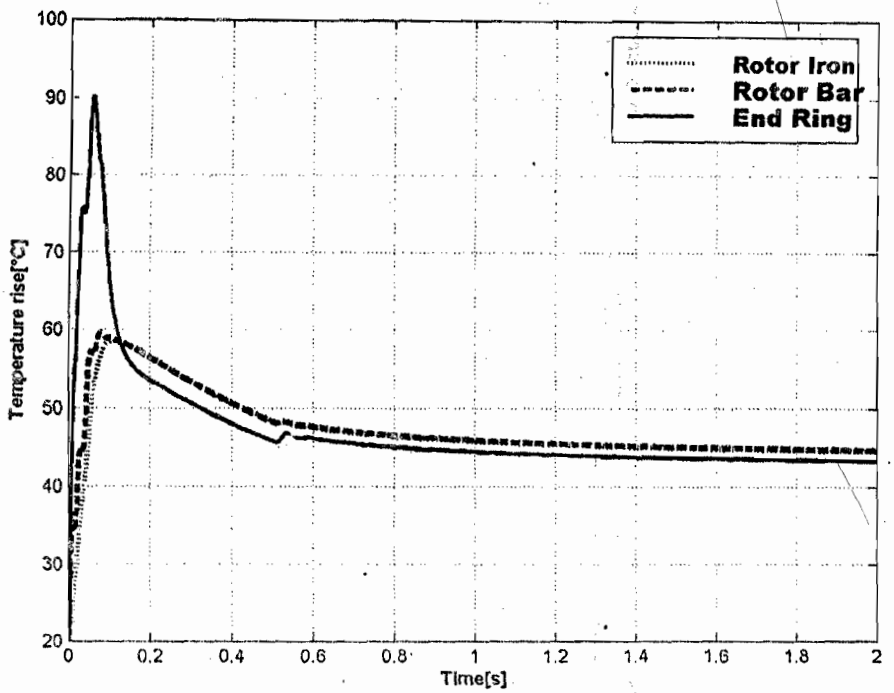

Figure 8: Graph of Temperature rise against Time

The power losses in the various parts of the test machine are depicted in figure 9, figure 10 and figure 11. Figure 12 shows the variation of stator and rotor resistances with time. The stator phase currents are shown in figure 13.

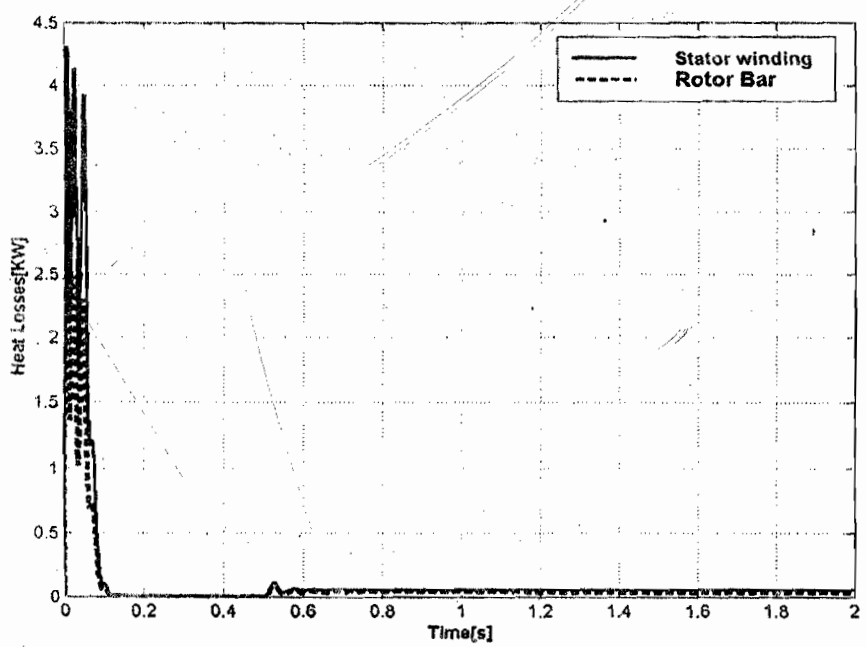

Figure 9: Graph of Power losses against Time

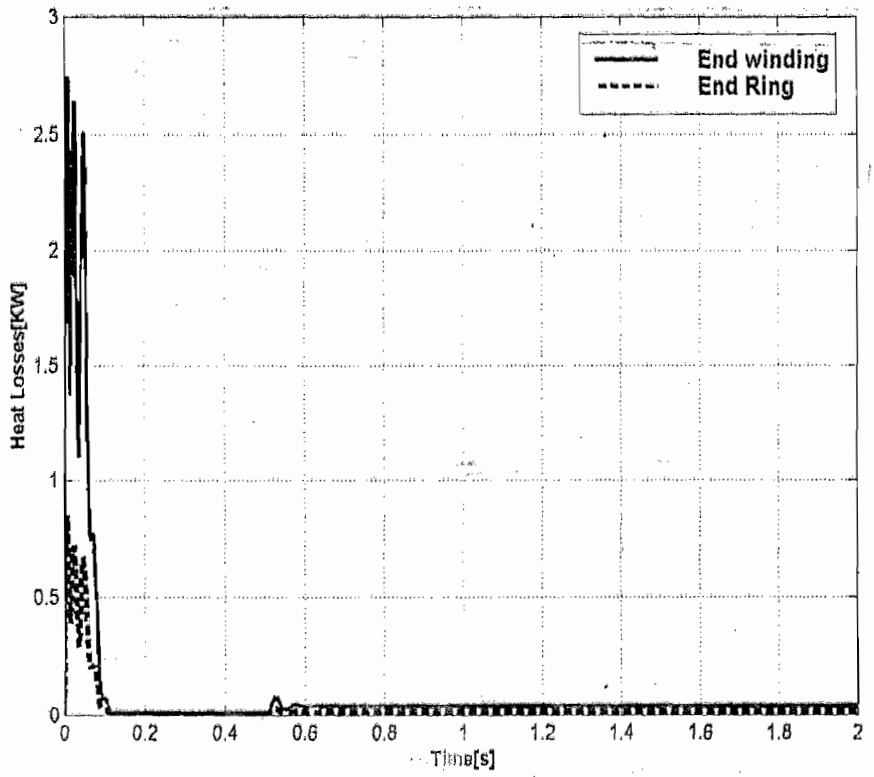

Figure 10: Graph of Power losses against Time

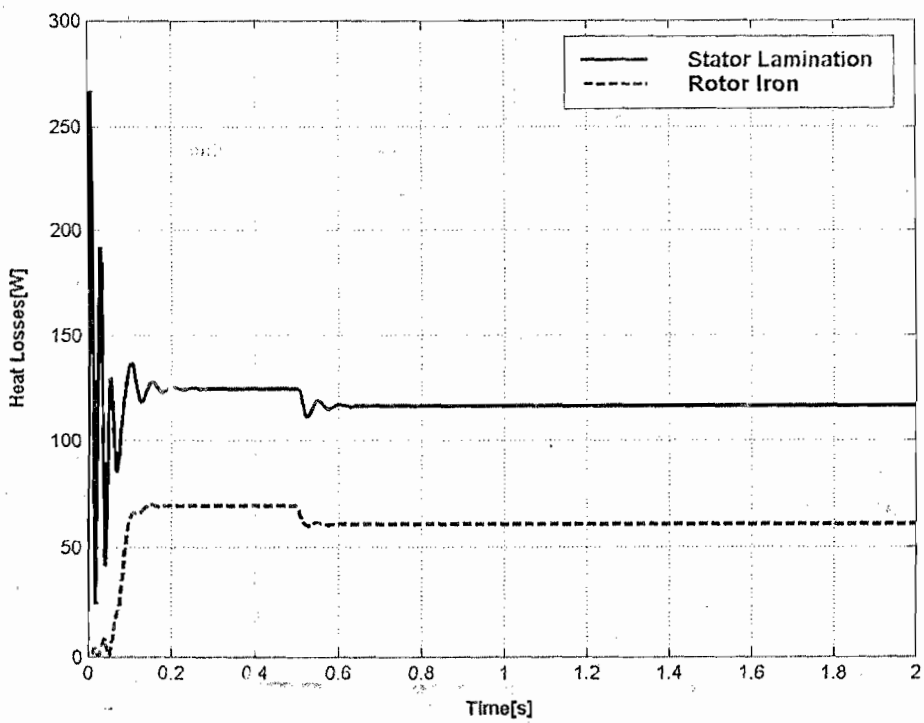

Figure 11: Graph of Power losses against Time

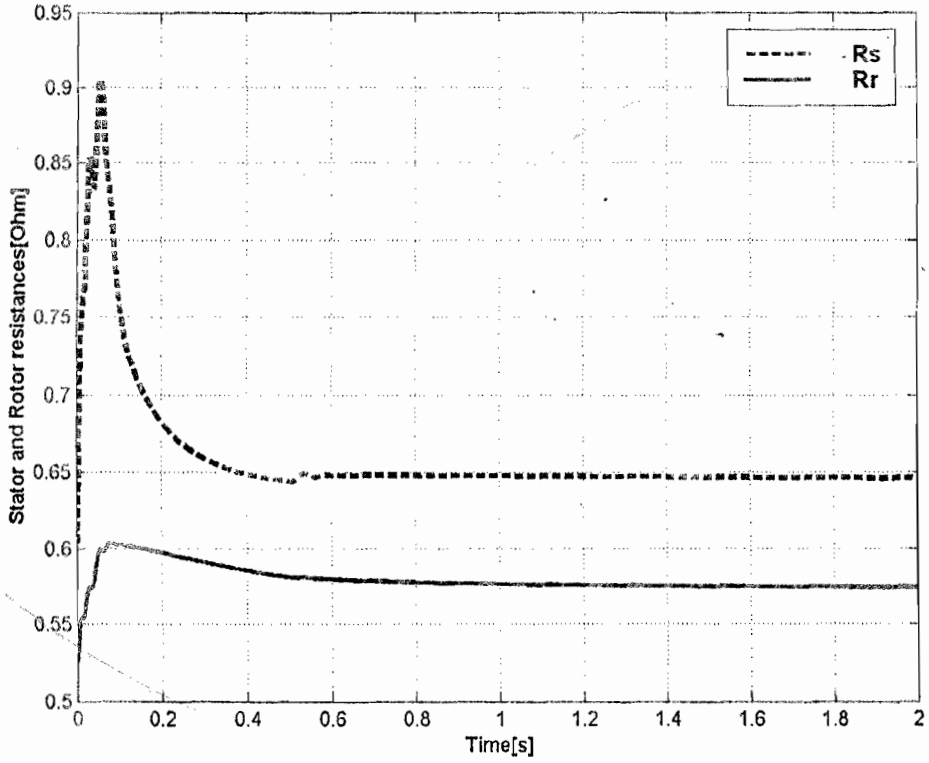

Figure 12: Graph of Stator and Rotor Resistances against Time

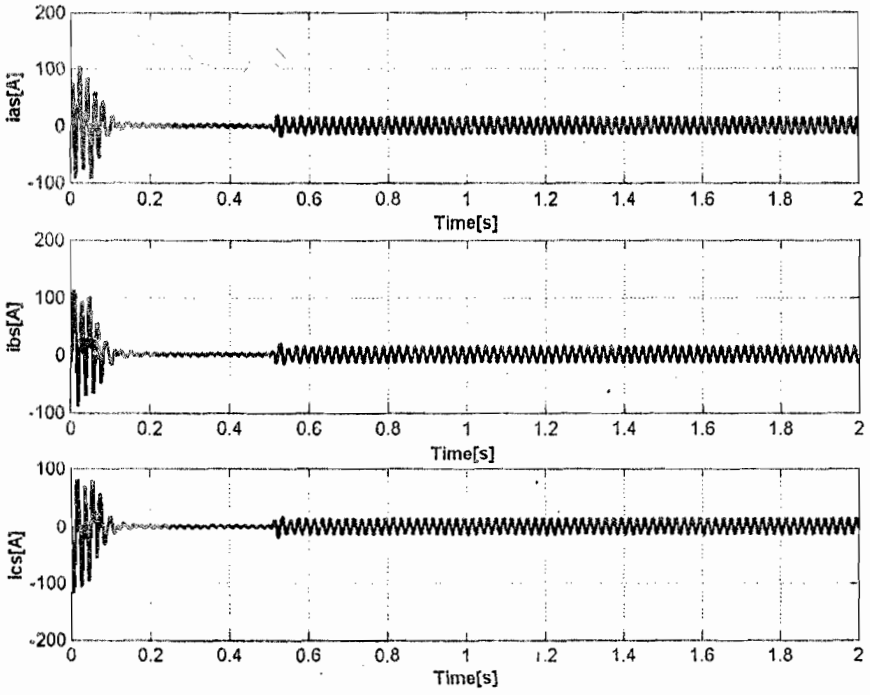

Figure 13: Graph of Stator Phase currents against Time

CONCLUSION AND OBSERVATIONS

The paper has presented a detail analysis and simulation of Electrical- Thermal coupling of induction machine. The results presented in this paper show that by studying the analysis of the coupled models, the overall behaviour of the induction machine—in terms of the thermal, electrical and mechanical transient behaviours can be predicted. This is in contrast to the conventional model which cannot be used to monitor the average temperatures of the different parts of the machine. In figure 7 it can be seen that at starting, the stator winding and the end winding average temperatures rise vary sharply within a short time interval. This is in contrast to figure 8 where the rotor iron and the rotor bar average temperature rises are sluggish. The trend of these graphs is understandable since in a squirrel-cage induction machine, actual winding exists in the stator which readily responds to the heat changes in the machine. Of interest also, is the steady state average temperatures of the test machine. Figure 8 shows that the steady state temperatures of the rotor iron and the rotor bar are higher than that of the stator winding and the end winding. The trend of figures(9-11) shows that great amount of heat is dissipated in the stator winding of the squirrel-cage induction machine.
By using these models and the results of the analysis, critical machine variables like currents, temperatures, torque and speed can be simultaneously monitored and controlled.

ACKNOWLEDGEMENT

The author wishes to express his thanks to DAAD for her financial support and to Prof. Dr.-Ing. B. Weidemann for his assistance in producing this paper.

REFERENCES

Bastos, J. P. ,Cabreira, M.F.R.R., Sadowski, N. and Arrunda, S. R., 1997. A thermal Analysis of induction motors using a weak coupled modeling. IEEE- Transactions on Magnetics, 33(2): 1714-1717.

Bousbane, A., McCormick, M. and Low, W. F., 1995. In-situ determination of thermal coefficients for electrical machines. IEEE transactions on Energy Conversion, 10(3): 385 –391.

Chan,C.C., Yan, L., Chen, P., Wang, Z. and Chau, K. T., 1994. Analysis of Electromagnetic and thermal fields for induction motors during starting. IEEE Transactions on Energy Conversion, 1:53-58.

Jordan, H. E., 1967. Digital Computer Analysis of induction machines in dynamic Systems. IEEE Transaction on power Apparatus and systems, PAS-86(6): 722-728.

Klamt, J., 1962. Berechnung and Bemessing elektrischer Maschinen. Springer Verlag.

Krause, P.C., 1986. Analysis of Electric Machinery New York, McGraw- Hill.

Krause, P.C. and Thomas. C. H., 1965. Simulation of symmetrical induction machinery. Transactions IEEE; PAS_84(11) :1038-1053.

Kylander, G., 1995. Thermal modelling of small cage induction motors Doctor of Technology Thesis, Chalmers University of Technology, Gothenburg, Sweden.

Mellor, P. H. , Roberts, D. and Turner, D. R., 1995. Lumped Parameter thermal model for electrical machines of TEFC design. IEEE Proc. B, 138 (5): 205-218.

Okoro, O. I., 2002. Dynamic and Thermal Modelling of Induction Machines with Non –linear Effects. Doctor of Engineering Thesis, University of Kassel, Germany.

Rajagopal, M.S., Seetharamu, K. N. and Ashwathnarayana, P.A., 1998. Transient thermal analysis of induction motors. IEEE Transactions on Energy Conversion, Vol.13, No13, No1, PP.62-69.

Rohrmoser, A., 1998. Entwarf einer Feldorientierten Regelung für einen doppeltgespeisten Asynchronmotor unter Berücksichtigung nichtlinearer Effekte. Diplomarbeit II, University of Kassel

Smith , A.C., 1996. A Transient induction motor model including saturation and deep bar effect. IEEE Transactions on Energy Conversion, 11(1): 8-15.

Smith, J. R., 1990. Response analysis of AC Electrical machines- Computer models and simulation. New York, John Willey and sons.

The MATLAB, 1997. The MATELAB Compiler User's guide, in Mathworks handbook. Math works.

The IEEE Standard, 1991. IEEE Standard Test Procedure for Polyphase induction motors and generators. IEEE Standard 112-1991.

Vas, Peter, 1992. Electrical Machines and Drives- A Space- Vector Theory Approach. Oxford, Clarendon Press.

APPENDIX A. MACHINE DATA

Output Power	7.5KW
Rated voltage	180V
Winding connection	Delta
Number of Poles	4
Rated speed	1495rpm
Rated frequency	50Hz
Stator resistance	0.601364Ω
Stator self inductance	1.87mH
Rotor resistance	0.5253Ω
Rotor self inductance	5.727mH
Magnetizing inductance	408.05mH
Mechanical Load torque	31.0N.m
Estimated rotor inertia moment	0.030382Kgm^2
Rated current	12.8A

Appendix B. Calculated thermal resistances and capacitances

Thermal capacitances	Values [J/K]	Thermal resistances	Values [K/W]
C_1	18446.55	R_{1b}	0.0416
C_2	4450.625	R_{12}	15.44e-3
C_3	423.388	R_{23}	35.58e-3
C_4	539.92	R_{26}	0.0.092
C_5	3204.08	R_{35}	0.1751
C_6	408.267	R_{48}	1.886
C_7	218.785	R_{67}	4.115e-3
C_8	1006	R_{79}	0.1055
		R_{78}	0.932
		R_{11c}	0.015